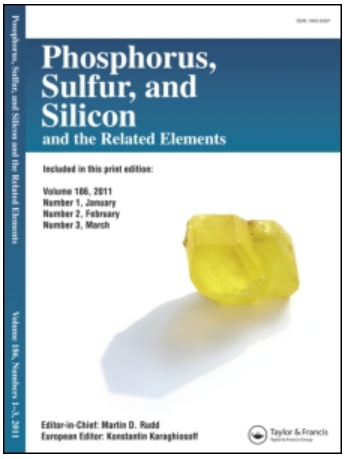

Phosphorus, Sulfur, and Silicon and the Related Elements

Publication details, including instructions for authors and subscription information:
http://www.informaworld.com/smpp/title~content=t713618290

Crystal Structure and Spectroscopic Investigations of a New Organic Monophosphate Monohydrate

H. Dhaouadi[a]; H. Marouani[a]; M. Rzaigui[a]; S. S. Al-Deyab[b]; A. Madani[c]
[a] Faculté des Sciences, Laboratoire de Chimie des Matériaux, Zarzouna, Bizerte, Tunisia [b] Petrochemical Research Chair, College of Science, King Saud University, Riyadh, Saudi Arabia [c] Faculté des Sciences, Laboratoire de Physique des Matériaux, Zarzouna, Bizerte, Tunisia

Online publication date: 24 February 2010

To cite this Article Dhaouadi, H. , Marouani, H. , Rzaigui, M. , Al-Deyab, S. S. and Madani, A.(2010) 'Crystal Structure and Spectroscopic Investigations of a New Organic Monophosphate Monohydrate', Phosphorus, Sulfur, and Silicon and the Related Elements, 185: 3, 609 — 619
To link to this Article: DOI: 10.1080/10426500902893191
URL: http://dx.doi.org/10.1080/10426500902893191

Phosphorus, Sulfur, and Silicon, 185:609–619, 2010

ISSN: 1042-6507 print / 1563-5325 online
DOI: 10.1080/10426500902893191

Taylor & Francis
Taylor & Francis Group

CRYSTAL STRUCTURE AND SPECTROSCOPIC INVESTIGATIONS OF A NEW ORGANIC MONOPHOSPHATE MONOHYDRATE

H. Dhaouadi,[1] H. Marouani,[1] M. Rzaigui,[1] S. S. Al-Deyab,[2] and A. Madani[3]

[1]*Laboratoire de Chimie des Matériaux, Faculté des Sciences, Zarzouna, Bizerte, Tunisia*
[2]*Petrochemical Research Chair, College of Science, King Saud University, Riyadh, Saudi Arabia*
[3]*Laboratoire de Physique des Matériaux, Faculté des Sciences, Zarzouna, Bizerte, Tunisia*

The chemical preparation, crystal structure, calorimetric study, and spectroscopic characterization are given for a new centrosymetric organic monophosphate monohydrate $(C_7H_{12}O_2NH_2)H_2PO_4{\cdot}H_2O$. This compound crystallizes in the orthorhombic Pbca unit-cell with a = 10.520(3) Å, b = 9.635(8) Å, c = 23.450(1) Å. The structure can be described as inorganic layers built by $H_2PO_4^-$ groups and H_2O molecules, parallel to ab planes, between which the organic groups $(C_7H_{12}O_2NH_2)^+$ are inserted. Multiple hydrogen bonds connect the different entities of the title compound giving rise to a three-dimensional network arrangement. Electrical conductivity measurements show that the $(C_7H_{12}O_2NH_2)H_2PO_4{\cdot}H_2O$ has a conductivity value that goes from $\sigma = 0.15 \times 10^{-6}\ \Omega^{-1}\ cm^{-1}$ at 338 K to $14.14 \times 10^{-6}\ \Omega^{-1}cm^{-1}$ at 429 K. Its characterization by TA, NMR, and IR also is reported.

Supplemental materials are available for this article. Go to the publisher's online edition of* Phosphorus, Sulfur, and Silicon and the Related Elements *to view the free supplemental file.

Keywords Crystal structure; hydrogen bonds; IR spectroscopy, thermal analysis; X-ray diffraction

INTRODUCTION

The chemistry of phosphates associated with organic cations that contain donor centers has received much attention because of their potential applications in various fields such as magnetism and ferro-electricity[1–3] and their rich structural chemistry. These hybrid compounds are also gaining importance in nonlinear optical applications.[4] These properties may result from the simultaneous presence of the organic species and the inorganic components. However, the use of a suitable organic molecule such as various amines and

Received 24 December 2008; accepted 13 March 2009.
Address correspondence to Houda Marouani, Laboratoire de Chimie des Matériaux, Faculté des Sciences, 7021 Zarzouna, Bizerte, Tunisie. E-mail: Houda.Marouani@fsb.rnu.tn

amino acids is expected to be a key factor in the formation of organic–inorganic hybrid compounds, which can adopt many structural arrangements with infinite one-, two-, and three-dimensional networks.[5–6] The structural properties of these hybrid materials are significantly influenced by the nature of the organic molecule, such as length, geometry, and the presence of functionalized groups. In this context, the series of organic phosphates exhibits rich structural and compositional diversity, presenting a particular crystal chemistry with weak and strong hydrogen bonds, as well as van der Waals forces taking part to stabilize the cohesion of these compounds.

To benefit from these materials, a good knowledge of their structural characteristics is fundamental, not only for the design of other hybrid compounds, but also for the prediction of their physicochemical properties. Results from X-ray crystallography, NMR spectroscopy, thermal analysis, IR spectroscopy, and impedance spectroscopy are combined to provide a good description of this new organic monophosphate $(C_7H_{12}O_2NH_2)H_2PO_4{\cdot}H_2O$. In particular, we report some results of the electric conductivity of the new organic monophosphate. The nature of this conductivity seems to be based on a Grotthuss mechanism of proton transport.

RESULTS AND DISCUSSION

Structural Description

The final atomic coordinates and thermal parameters of all non hydrogen atoms of $(C_7H_{12}O_2NH_2)H_2PO_4{\cdot}H_2O$ are given in Table S1 (available online in the Supplemental Materials). Interatomic distances and bond angles are given in Table I.

As seen in the ORTEP view (Figure 1), the asymmetric unit corresponds to the formula unit, which is built of three entities: the $H_2PO_{4^-}$ anion, the H_2O molecule, and the organic cation $C_7H_{12}O_2NH_2{}^+$.

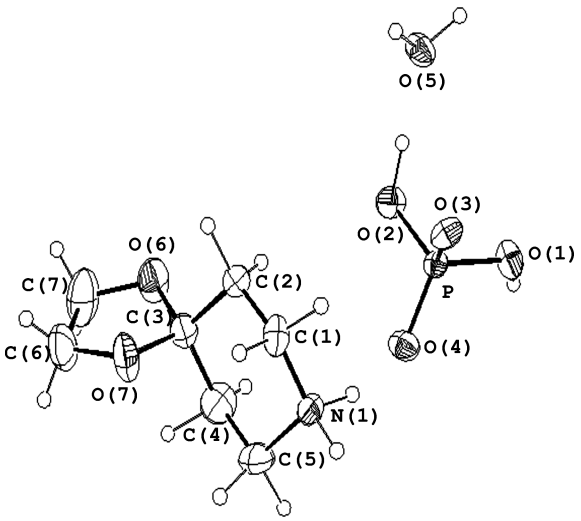

Figure 1 ORTEP view of the structure of $(C_7H_{12}O_2NH_2)H_2PO_4{\cdot}H_2O$ (50% thermal ellipsoids).

Table I Main interatomic distances (Å) and angles (°) in $(C_7H_{12}O_2NH_2)H_2PO_4{\cdot}H_2O$ atomic arrangement

The PO_4 tetrahedron				
P	O(1)	O(2)	O(3)	O(4)
O(1)	**1.565 (2)**	2.518 (3)	2.503 (2)	2.467 (2)
O(2)	107.3 (1)	**1.562 (2)**	2.410 (3)	2.528 (2)
O(3)	109.4 (1)	103.5 (1)	**1.504 (2)**	2.539 (2)
O(4)	108.1 (1)	111.9 (1)	116.3 (1)	**1.484 (2)**
O(1)−H(O1)	1.02 Å	P−O(1)−H(O1)	115.7 °	
O(2)−H(O2)	0.84 Å	P−O(2)−H(O2)	116.2 °	
P···P = 4.367(5) Å				
$[C_7H_{12}O_2NH_2]^+$ group				
N−C(1)	1.489(4)	N−C(1)−C(2)	110.1(2)	
C(1)−C(2)	1.503(4)	C(1)−C(2)−C(3)	111.5(2)	
C(2)−C(3)	1.492(4)	C(2)−C(3)−C(4)	109.2(2)	
C(3)−C(4)	1.504(5)	C(3)−C(4)−C(5)	112.4(3)	
C(4)−C(5)	1.487(5)	C(4)−C(5)−N	110.3(3)	
C(5)−N	1.480(4)	C(5)−N−C(1)	112.0(2)	
C(3)−O(6)	1.412(3)	C(2)−C(3)−O(6)	109.8(2)	
C(7)−O(6)	1.404(5)	C(2)−C(3)−O(7)	109.3(2)	
C(7)−C(6)	1.462(6)	C(4)−C(3)−O(7)	111.7(2)	
O(7)−C(6)	1.400(4)	O(6)−C(3)−O(7)	105.4(2)	
O(7)−C(3)	1.418(3)	O(6)−C(7)−C(6)	106.9(3)	
		C(7)−C(6)−O(7)	105.8(3)	
		C(6)−O(7)−C(3)	108.9(2)	
		O(6)−C(3)−C(4)	111.3(2)	
		O(7)−C(3)−C(2)	109.3(2)	

Hydrogen bonds geometry: Bond lengths (Å) and angles (°)

D—H···A	D−H	H···A	D···A	D−H···A
O1−H(O1)···O(W)	1.02	1.59	2.603(3)	175.4
O2−H(O2)···O(3)	0.84	1.78	2.570(3)	156.4
OW−H(1W)···O(4)	0.99	1.73	2.716(3)	175.7
OW−H(2W)···O(3)	0.94	1.87	2.789(2)	165.8
N−H(1N)···O(3)	0.93	1.95	2.861(3)	163.5
N−H(2N)···O(4)	1.01	1.75	2.727(3)	163.0
		H(1W)−OW−H(2W)	103.2	

Estimated standard deviations are given in parentheses.

The structure can be described as inorganic layers built up with $H_2PO_4^-$ anions and water molecules, parallel to the *ab* planes around z = 1/4 and z = 3/4 planes. The organic cation is located between these layers (Figure S1, Supplemental Materials).

Examination of the $H_2PO_4^-$ geometry (Table I) shows two types of P−O distances. The largest ones, 1.565 (2) Å and 1.562 (2) Å, can be attributed to the P−OH distances, while the shortest ones, 1.504 (2) Å and 1.484 (2) Å, correspond to the phosphoric atom doubly bonded to the oxygen atom (P=O). The average values of the P−O distances and O−P−O angles are 1.529 Å and 109.4°, respectively. These similar geometrical features have also been noticed in other crystal structures.[7–8] Nevertheless, the calculated average values of the distortion indices[9] corresponding to the different angles and distances in

the PO_4 tetrahedron [DI(PO) = 0.022, DI(OPO) = 0.029, and DI(OO) = 0.015] show a pronounced distortion of the PO distances and OPO angles if compared to O—O distances. However, these indices are in good agreement with the overall mean values obtained for H_nPO_4 (n = 1, 2) groups. The tetrahedron PO_4 is then described by a regular oxygen atom arrangement with the P atom slightly shifted from the gravity center of PO_4.

The interconnection between two adjacent anions $H_2PO_4^-$ is assured by a strong H-bond [d (O···O) < 2.73 Å][10] to form infinite chains that spread along the *b* direction. It is worth noting that the O···O distances involved in the hydrogen bonds [2.568(3)–2.603(3) Å] are of the same order of magnitude as the O···O distances in the H_2PO_4 tetrahedron [2.410(3)–2.539(2) Å]. These distances and the short P···P one of 4.367(5) Å allow us to consider the $[H_2PO_4]_n^{n-}$ network as a polyanion.

The $H_2PO_4^-$ group connects three H_2O molecules and four cationic groups by the hydrogen bonds. It is worth noting that H_2O molecules do not have any hydrogen-bonding interaction with ($C_7H_{12}O_2NH^+_2$) groups. From Figure S2 (Supplemental Materials), it can be seen that one H_2O molecule links three $(H_2PO_4)^-$, groups and one $(H_2PO_4)^-$ group links three H_2O molecules by the interaction of hydrogen bonds to perform an infinite two-dimensional network.

Hydrogenphosphate chains can show a great variety of hydrogen bonding motifs. In 2-(2-ammonium ethyl ammonium) ethanol monohydrogenmonophosphate monohydrate,[11] infinite chains of HPO_4^{2-} groups are linked by single P—O—H···O—P connections, while in triethanolammonium dihydrogenphosphate,[12] the $H_2PO_4^-$ entities are connected by alternating single and double P—O—H···O—P hydrogen-bond links. The 2-aminopyridinium dihydrogenphosphate[13] contains a double tetrahedral chain different from that seen in the title compound. The comparison of the hydrogen bond scheme in these compounds shows that this scheme is strongly affected by the nature of the organic molecule and the presence of crystallization water molecule.

As shown in Figure S1, each organic cation is linked to two anionic chains by one type of hydrogen bond, N-H···O. The hydrogen bonds N-H···O range from 1.75 Å to 1.95 Å in O···H length with N-H···O angles between them [163°–163.5°] (Table I). All the hydrogen bonds, the van der Waals contacts, and electrostatic interactions between the different entities give rise to a three-dimensional network in the structure and add stability to this compound. The organic cations are localized in the interlayer spacing and organized in opposite orientation along the *c*-axis (Figure 2). The main geometrical features of organic cations are given in Table I. The organic cation exhibits a regular spatial configuration with usual distances C—C, C—N, C—O, C—C—C, C—C—N, C—C—O, C—N—C, and C—O—C angles. The organic molecule contains two rings, joined at the C(3) atom. The first ring [C(1)—C(2)—C(3)—C(4)—C(5)—N(1)] presents a chair conformation, while the second one [C(3)—O(6)—C(7)—C(6)—O(7)] shows a planar part that contains the two oxygen atoms O(6) and O(7).

NMR Spectroscopy

Figure 2 shows the proton decoupled ^{31}P MAS–NMR spectrum of crystalline monophosphate $(C_7H_{12}O_2NH_2)H_2PO_4{\cdot}H_2O$. It exhibits only one sharp peak, related to the single phosphorus environment that exists in the atomic arrangement. The corresponding chemical shift value −0.37 ppm agrees with those of monophosphate (between −10 and +5 ppm), depending on the compound.[14–19] This single peak is in good agreement with the X-ray results.

Table II Crystal data and experimental parameters used for the data collection, strategy, and final results of the structure determination

I: Crystal data	
Formula: $C_7H_{18}NO_7P$	Fw = 259.20
System: orthorhombic	Space group: Pbca
a = 10.520(3) Å, b = 9.635(8) Å, c = 23.45(1) Å	
Z = 8	Volume = 2377 (2) $Å^3$
Refinement of unit cell parameters with 25 reflections	($8° < \theta < 10°$)
$\rho_{cal.} = 1.449$ g.cm^{-3}	F (000) = 1104.00
Linear factor absorption:	μ (AgK_α) = 1.38 cm^{-1}
Crystal size: (0.8 × 0.6 × 0.35) mm^3	Colour: colorless
Morphology: prism	
II: Intensity measurements	
Diffractometer: Enraf-Nonius MACH 3	Wave length: AgK_α (0.5608 Å)
Temperature: 296.2 K	Scan width: 1.20°
Scan mode: $\omega/2\theta$	thêta (θ) range: 2.05–24.96°
Measurement area: $0 < h < 15$, $0 < k < 14$, $-35 < l < 0$	
Nb of scanned reflections: 4827	
Nb of independent reflections: 4769	
III: Structure determination	
Unique reflection included: 2114 with $I > 3\sigma$ (I)	Refined parameters: 145
Weighting scheme: $1/[\sigma^2 (F_0) + 0.00027 (F_0)^{2}]$	
Residual Fourier density:	$-0.22 < \rho < 0.34$ e.$Å^{-3}$
Unweighted R factor: R = 0.047	Weighted R factor = 0.052
Esd: 1.72	Δ/σ (max) = 0.01

The ^{13}C CP-MAS NMR spectrum of the title compound displays four different peaks with variable intensities (Figure S3, Supplemental Materials). The carbon atoms of the organic group are labeled as depicted below. This spectrum shows that carbon atoms C6 and C7 are magnetically equivalent, giving the single peak at 65.8 ppm. Their chemical

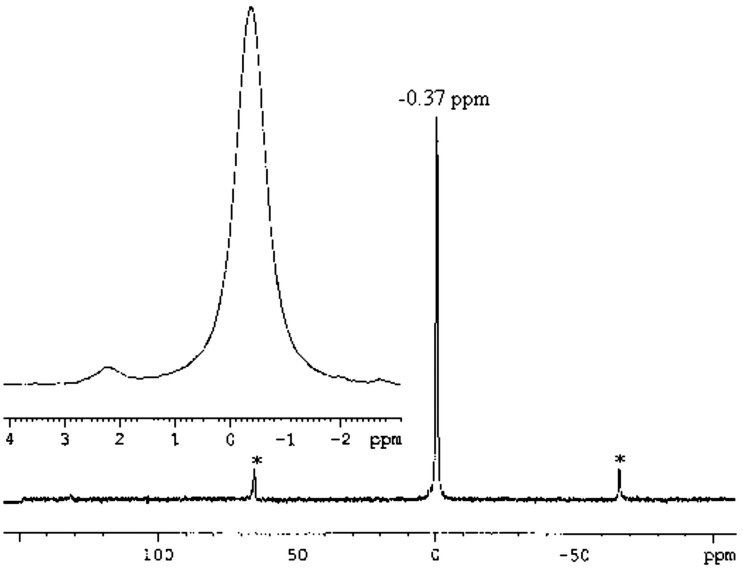

Figure 2 ^{31}P MAS-NMR spectrum of $(C_7H_{12}O_2NH_2)H_2PO_4 \cdot H_2O$ recorded at 4 kHz. *Spinning side bands.

shifts are relatively important, due to the fact that they are directly bonded to the two oxygen atoms. The C3 carbon atom, which is bound to two oxygen atoms, exhibits the important chemical shift (105.2 ppm) in comparison to the other carbon atoms of the organic cation. The equivalence of the C2 and C4 as well as C1 and C5 atoms could be the results of the environment effect. The experimental data for ^{13}C are summarized in Table S2 (Supplementary Materials). These results prove the presence of only one organic cation in the asymmetric unit of the compound, in good agreement with the X-ray study.

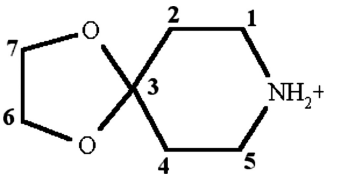

IR Spectroscopy

The infrared absorption spectrum of the title compound reported in Figure S4a (Supplementary Materials) shows vibrations band characteristic of the organic cation, the $H_2PO_4^-$ anion, and the water molecule. The assignment attempts are based on previous results encountered in the literature[20–22] and on the predictions of group theoretical analysis. The valency vibrations of the organic group in its protonated form appear between 3400–2500 and 1650–1300 cm^{-1}. Various valency and bending vibration bands, whose number and positions are between 1200 and 300 cm^{-1}, are both characteristic of a monophosphoric anion. In this type of anion, these vibrations are expected to appear in the 1200–800 and 650–300 cm^{-1} ranges, respectively. The bands observed in the IR spectrum in the 1260–1200 cm^{-1} region are ascribed to the δ_{P-O-H} in plane bending, and the γ_{P-O-H} out of plane bending modes appear in the range 900–800 cm^{-1}. The presence of a strong band at 1650 cm^{-1} is assigned to the bending vibration modes of the H_2O molecule. Multiple bands extending from 3400 to 2500 cm^{-1} are observed in the IR spectrum. These bands are due to the symmetric and asymmetric stretching modes of H_2O, NH_2, CH_2, and OH. Frequencies in the range 1700–1300 are attributed to $\delta(H_2O)$ $\delta(NH_2)$, $\delta(CH_2)$, and δ(OH) bending vibrations.

Thermal Behavior

Figure S5 (Supplemental Materials) shows that both TGA and DTA thermograms of the hybrid compound heated from room temperature to 723 K. From these curves, we deduce that the thermal decomposition occurs in two stages. The first one corresponds to the removal of the water molecule (weight loss calculated 6.94%, observed 6.89%) in the temperature range 348–413 K; it is related to the two endothermic peaks on the DTA curve at 357 and 406 K. The strength of the hydrogen bonds in the network explains the removal of the water molecule in this large temperature range. This situation is also observed in other hydrate phosphates such as $(C_4H_{14}N_2O)HPO_4{\cdot}H_2O$,[23] in which the removal of the water molecule is observed in the temperature range 364–443 K.

The second process related to the other endothermic peak observed in the DTA at 503 K is a combination of a melting and a degradation of the obtained phase. The TGA curve

shows continuous weight loss corresponding to the departure of the degradation products. The resulting compound is a consistent viscous residue, probably formed of polyphosphoric acids and black carbon.

A typical result of the calorimetric study on the organic phosphate is represented in Fig. S6 (Supplemental Materials), which shows the diagram obtained while heating a recently prepared sample of $(C_7H_{12}O_2NH_2)H_2PO_4{\cdot}H_2O$ in the temperature range (293–723 K). The sample was heated in open air at heating rate of 5 K.min^{-1}. The obtained curve exhibits the three strongest endothermic peaks around 356 K, 394 K, and 498 K. The first two thermal events, at about 356 K and 394 K, can be attributed to the departure of the water molecule intercalated in the structure. These two peaks are well observed in the DTA curve in the same temperature range. In order to examine the nature of this transformation between 356–394 K, an investigation by IR absorption was undertaken. In fact, the IR spectrum (Figure S4b, Supplemental Materials) of the sample heated at 423 K and then cooled showed the disappearance of the broad band around 3500 cm^{-1} and distinct changes for the absorption around 1600 cm^{-1} attributed to the stretching and the bending vibration modes, respectively, of the water molecule. These experimental facts indicate the departure of the water molecule in a large temperature range. The third endothermic peak present at 498 K corresponds to the melting and the degradation of the obtained compound.

Electrical Conductivity Analysis

Some complex impedance diagrams Im. Z (Ω) versus Real Z (Ω) recorded at various temperatures are given in Figure S7 (Supplemental Materials). The conductivity σ of was calculated using the following equation $\sigma = \frac{d}{AR}$, where d, A, and R represent the thickness, the area, and the resistance, respectively. The resistance was obtained from the intercept of the Nyquist plot with the real axis. The Nyquist plot does not show any semicircle up to 338 K, since until this temperature the resistance of the sample is still greater than 1 MOhm, the limit of the HP analyzer. But as the temperature is increased, a clear semicircle is observed. All these semicircles merge and terminate on the real impedance axis at higher frequency side. This indicates the presence of only one bulk resistance for this material, and the grain boundary resistance is negligibly small as no second semicircle is observed.

The temperature dependence of the conductivity between 338 K and 429 K is represented in Figure S8 (Supplementary Materials) in the form of Ln (σT) versus 10^4/T. In this range of temperature, the electrical conductivity increases with increasing temperature. However, at low temperature (338–368 K), the conductivity has approximately an Arrhenius type behavior $\sigma = \frac{A}{T}\exp(\frac{-Ea}{KT})$, where A is a constant depending on the material, K the Boltzmann constant, and Ea the activation energy determined by the slope of the interpolating Arrhenius curve ($Ea = 0.27$ eV). Starting at temperature 368 K, a break in the curve is observed, accompanied at high temperature by increasing activation energy ($Ea = 0.95$ eV). This change in slope can be coupled to the removal water; the obtained compound is anhydrous, which can favor another type of conductivity mechanism. These results are in good agreement with calorimetric study, which shows the departure of the water molecule in the same temperature range, giving thus an anhydrous compound.

On the basis of our experimental results and the date in the literature, the electric properties of this hybrid compound may be interpreted by the following way: The increase in temperature can favor the vibration of the inorganic layers, which induce a rapid reorientation $H_2PO_4^-$ and fast moving H^+.[24] The fact that the −OH groups belonging to the monophosphate anions form infinite layers is strongly in favor of a protonic mobility in the

structure. Indeed, the $H_2PO_4^-$ anion performs both as proton donor and acceptor, by its four oxygen atoms, thus producing an extended intermolecular H-bond network, through which structural migration of the proton may occur via Grotthuss mechanism.[25] This mechanism is proposed for proton conductivity in phosphoric acid–doped polybenzimidazole[25] and for $K_4(SO_4)(HSO_4)_2(H_3AsO_4)$.[26] In a superprotonic phase of $K_2(HSeO_4)_{1.5}(H_2PO_4)_{0.5}$,[27] protons diffuse by the Grotthuss mechanism, which is a cooperative process involving proton-displacement and reorientation of the PO_4 entities. We suggest that the proton migrates from a site to a neighboring vacant one. In the present case, when the temperature increases, the hydrogen bonds become progressively weaker, such that the protons start to jump from an oxygen atom of the PO_4 tetrahedra to another one, and the PO_4 group adopts new reorientations, which cause the formation of a new hydrogen bond.[28]

The same range of ionic conductivity and activation energy were found for the other phosphate compounds such as $Pb_2Bi(V_{0.84}P_{0.16})O_6$ ($\sigma_{300K} = 1.34\ 10^{-7}\ \Omega^{-1}cm^{-1}$, Ea = 0.92 eV).[29]

In order to understand the structural mechanism of the protonic conductivity in the $(C_7H_{12}O_2NH_2)H_2PO_4{\cdot}H_2O$, the electrical response of the material has been analyzed by complex modulus M*(ω) formalism.[30] The complex modulus defined as $M^* = i\omega C_0 Z$, where C_0 is the vacuum capacitance of the measuring cell, $\omega = 2\pi f$ and $i^2 = -1$, can provide useful information about the relaxation process of the dipolar group such as $H_2PO_4^-$. For a given temperature and frequency, the real part (M′) and the imaginary part (M″) of the M* complex modulus (M* = M′ + j M″) have been calculated from the complex data (Z* = Z′—jZ″) using the relations $M' = \omega C_0\ Z''$ and $M'' = \omega C_0\ Z'$. A plot of log M′ and the normalized M''/M''_{max} imaginary part of the complex modulus versus Log f are given in Figures S9 and S10 (Supplementary Materials) at various temperatures for the $(C_7H_{12}O_2NH_2)\ H_2PO_4{\cdot}H_2O$ material. As seen in Figure S9 for all temperatures given, the value of M′ reaches a maximum at high frequencies. At low frequencies, it decreases sharply, which indicates that the electrode polarization phenomena make a negligible contribution to M*(ω) and may be ignored when the electric data are analyzed in this form.[31]

In Figure S10, we introduce the ($M''/M''_{max.}$) dependence of (log f) relative to a given temperature. When the temperature increases, the modulus peak maximum shifts to higher frequencies (Figure S10). Observation of the M''/M''_{max} plots shows the absence of any additional peaks at lower frequencies, which indicates negligible contribution of grain boundary and electrode effects to the total conductivity. The f_p frequency relative to M''_{max} peak ($f_p = 1/2\pi\tau_\sigma$) is defined by the condition $\omega\tau_\sigma = 1$, where τ_σ is the most probable proton relaxation time, and f_p shifts upward with increasing temperature. This relaxation process seems to originate probably from the proton jump and the phosphate reorientation. Such an interpretation has been adopted for many solid electrolytes such as $(C_6H_5CH_2C_5H_4NH)H_2PO_4$,[32] KH_2PO_4,[33] and $NH_4H_2PO_4$.[34]

CONCLUSION

The use of the protonated 1,4 dioxa-8-azaspiro(4,5)decane $C_7H_{12}O_2NH$ as organic cation in the phosphate matrix leads to a new hybrid compound of the chemical formula $[C_7H_{12}O_2NH_2]H_2PO_4{\cdot}H_2O$. The crystal structure of this compound was found to be built by infinite layers of $H_2PO_4^-$ anions and H_2O molecules parallel to the *ab* plane around $z = \frac{1}{4}$ and $z = \frac{3}{4}$. Between these layers the organic molecules are stacked parallel to *b* direction. Both the organic and inorganic components perform different interactions (electrostatic,

Van der Waals, H-bonds) to stabilize the three-dimensional network. From impedance measurements, both the conductivity and modulus spectrum of this compound were analyzed at low and high frequencies in the 338–429 K temperature range. These curves show the temperature dependence of resistance, proving that the most probable mechanism of the proton conductivity of the title compound was the so-called Grotthus mechanism, which arises from protons jumping between the nitrogen, the phosphate oxygen, and the water molecule. Solid-state ^{31}P and ^{13}C MAS-NMR spectroscopies are in accordance with the X-ray structure.

EXPERIMENTAL

Chemical Preparation

Crystals of the title compound $(C_7H_{12}O_2NH_2)H_2PO_4{\cdot}H_2O$ were prepared by slowly adding, at room temperature, concentrated orthophosphoric acid H_3PO_4 [0.55 mL, 85% wt, d = 1.7] to an aqueous solution containing 1,4-dioxa-8-azaspiro(4,5)decane $C_7H_{12}O_2NH$ [1.25 mL, 98% wt, d = 1.1]. Acid was added under continuous stirring. A white precipitate formed, and then phosphoric acid was added until it disappeared. Schematically the reaction can be written as follows:

$$C_7H_{12}O_2NH + H_3PO_4 + H_2O \rightarrow (C_7H_{12}O_2NH_2)H_2PO_4.H_2O$$

The obtained solution was slowly evaporated at room temperature for several days until the formation of transparent prismatic single crystals of good quality and suitable dimensions for crystallographic study (1.5 g, 60% yield). The crystals obtained in this way are stable for a long time under normal conditions of temperature and humidity. The chemical formula of this new material, $(C_7H_{12}O_2NH_2)H_2PO_4{\cdot}H_2O$, was determined by X-ray crystal structure analysis.

Investigation Techniques

The title compound has been studied by various physicochemical methods:

X-Ray Diffraction. The intensity data collection was performed using a MACH3 Enraf-Nonius diffractometer. The experimental conditions of data collection, the strategy followed for the structure determination, and its final results are given in Table II.

Crystallographic data (CIF) for the structure reported in this article have been deposited with the Cambridge Crystallographic Data Center as supplementary publication CCDC 714462. Copies of the data can be obtained, free of charge, upon application to the CCDC, 12 Union Road, Cambridge CB12EZ, UK (Fax: +44(1223)336-033; e-mail: deposit@ccdc.cam.ac.uk).

NMR Spectroscopy. The NMR spectra were recorded on a Bruker DSX-300 spectrometer operating at 121 MHz for ^{31}P and 75.49 MHz for ^{13}C. All measurements were carried out at room temperature, with H_3PO_4 (85%) as an external standard reference. Phosphorus spectra were recorded under classical MAS conditions, while the carbon ones were recorded by use of cross-polarization from protons.

Thermal Behavior. Thermal analysis was performed using the Multimodule 92 Setaram analyzer operating from room temperature up to 723 K at an average heating rate of 5 K min^{-1}.

Infrared Spectroscopy. IR spectra were recorded in the range 4000–400 cm^{-1} with a Perkin-Elmer FTIR spectrophotometer 1000 using samples dispersed in spectroscopically pure KBr pellet.

Electrical Conductivity. Conductivity measurements were carried out on a pressed powder in the frequency range of 10 Hz to 13 MHz, with an applied voltage of 10 mV. Sample pellets, 13 mm in diameter and 1.5–2.0 mm in thickness, were made by pressing 200–400 mg of the hybrid material $(C_7H_{12}O_2NH_2)H_2PO_4{\cdot}H_2O$ under a pressure of 12 tons for 1 min, at room temperature. Metallic silver was deposited on both sides, which served as electrodes. The pellet was placed between two blocking electrodes in a tubular furnace, submitted to a temperature regulator. The conductivity was then measured from room temperature to 429 K, with 5–15 K steps, by checking the complex impedance spectroscopy with a Hewlett-Packard 4129A impedance analyzer.

REFERENCES

1. R. Masse, M. Bagieu-Beucher, J. Pecaut, J. P. Levy, and J. Zyss, *Nonlinear Opt.*, **5,** 413 (1993).
2. A. I. Baranov, B. V. Merinov, A. V. Tregubchenko, and L. A. Shuvalov, *Ferroelectrics*, **81,** 1151 (1988).
3. A. I. Baranov, A. V. Tregubchenko, L. A. Shuvalov, and N. M. Shchagina, *Sov. Phys. Solid State*, **29,** 1448 (1988).
4. J. Zyss, J. Pecaut, J. P. Levy, and R. Masse, *Acta Crystallogr.*, **B49,** 334 (1993).
5. M. T. Averbuch-Pouchot, A. Durif, and J. C. Guitel, *Acta Crystallogr.*, **C44,** 99 (1988).
6. M. T. Averbuch-Pouchot, A. Durif, and J. C. Guitel, *Acta Crystallogr.*, **C45,** 421 (1989).
7. L. Baouab, T. Guerfel, M. Soussi, and A. Jouini, *J. Chem. Crystallogr.*, **30,** 805 (2000).
8. B. K. Aoki, K. Nagano, and Y. Iitaka, *Acta Crystallogr.*, **B27,** 11 (1971).
9. W. H. Baur, *Acta Crystallogr.*, **B30,** 1195 (1974).
10. I. D. Brown, *Acta Crystallogr.*, **A32,** 24 (1976).
11. L. Ben Hamada and A. Jouini, *Mater. Res. Bull.*, **40,** 459 (2005).
12. S. Demir, V. T. Yilmaz, O. Andac, and W. T. A. Harrrison, *Acta Crystallogr.*, **E59,** 907 (2003).
13. S. Demir, V. T. Yilmaz, and W. T. A. Harrrison, *Acta Crystallogr.*, **C61,** 565 (2005).
14. A. R. Grimmer and U. Haubenreisser, *Chem. Phys. Lett.*, **99,** 487 (1983).
15. D. Mûller, E. Jahn, G. Ladwig, and U. Haubenreisser, *Chem. Phys. Lett.*, **109,** 332 (1984).
16. A. K. Cheetham, N. J. Clayden, C. M. Dobson, and R. J. B. Jakemen, *J. Chem. Soc., Chem. Commun.*, **4,** 195 (1986).
17. L. Mudracovskii, V. P. Shmochkova, N. S. Kentsarenko, and V. M. Mastikhin, *Phys. Chem. Solids*, **47,** 335 (1986).
18. G. L. Turner, K. A. Smith, R. J. Kirkpatrick, and E. J. Oldfield, *Magn. Reson.*, **70,** 408 (1986).
19. S. Prabhakar, K. J. Rao, and C. N. R. Rao, *Chem. Phys. Lett.*, **139,** 96 (1987).
20. K. Nakamoto, *Infrared and Raman Spectra of Inorganic and Coordination Compounds*, 4th ed. (Wiley-Interscience, New York, 1986).
21. C. Livage, C. Egger, and G. Férey, *Chem. Mater.*, **11,** 1546 (1999).
22. K. Kaabi, A. Rayes, C. Ben Nasr, M. Rzaigui, and F. Lefebvre, *Mater. Res. Bull.*, **38,** 741 (2003).
23. L. Ben Hamada and A. Jouini, *Mater. Res. Bull.*, **40,** 459 (2005).
24. N. Zouari, H. Khemakhem, T. Mhiri, and A. Douad, *J. Phys. Chem. Solids*, **60,** 1779 (1999).
25. A. Schechter and R. F. Savinell, *Solid State Ionics*, **147,** 181 (2002).
26. M. Amri, N. Zouari, T. Mhiri, S. Pechev, P. Gravereau, and R. Von Der Muhll, *J. Phys. Chem. Solids*, **68,** 1281 (2007).
27. N. Zouari, K. Jaouadi, and T. Mhiri, *Solid State Ionics*, **177,** 244 (2006).
28. J. E. Diorsa, R. A. Vargas, I. Albinson, and B.-E. Mellander, *Solid State Ionics*, **177,** 1107 (2006).

29. O. Labidi, P. Roussel, M. Huve, M. Drache, P. Conflant, and J. P. Wignacourt, *J. Solid State Chem.*, **178,** 2247 (2005).
30. S. Lanfredi, P. S. Saia, R. Lebullenger, and A. C. Hernaldes, *Solid State Ionics*, **146,** 329 (2002).
31. F. S. Howell, R. A. Bose, P. B. Macedo, and C. T. Moynihan, *J. Phys. Chem.*, **78,** 639 (1974).
32. I. Ben Djemaa, Z. Elaoud, T. Mhiri, R. Abdelhedi, and J.-M. Savariault, *Solid State Commun.*, **142,** 610 (2007).
33. J. E. Diorsa, R. A. Vargas, I. Albinson, and B.-E. Mellander, *Phys. Status Solid*, **B241,** 1369 (2004).
34. J. E. Diorsa, R. A. Vargas, I. Albinson, and B.-E. Mellander, *Solid State Commun.*, **132,** 55 (2004).